Cancer Cell International

RESEARCH

Open Access

Integrative analysis of aging-related genes reveals CEBPA as a novel therapeutic target in non-small cell lung cancer

Jiaqi Zhu[1†], Xiaoren Zhu[2†], Conglin Shi[3†], Qixuan Li[1], Yun Jiang[4], Xingyou Chen[5], Pingping Sun[6], Yi Jin[7*], Tianyi Wang[1*] and Jianle Chen[1*]

Abstract

Background To explore the impact of ARGs on the prognosis of NSCLC, and its correlation with clinicopathological parameters and immune microenvironment. Preliminary research on the biological functions of CEBPA in NSCLC.

Methods Using consensus clustering analysis to identify molecular subtypes of ARGs in NSCLC patients; employing LASSO regression and multivariate Cox analysis to select 7 prognostic risk genes and construct a prognostic risk model; validating independent prognostic factors of NSCLC using forest plot analysis; analyzing immune microenvironment correlations using ESTIMATE and ssGSEA; assessing correlations between prognostic risk genes via qPCR and Western blot in NSCLC; measuring mRNA and protein expression levels of knocked down and overexpressed CEBPA in NSCLC using CCK-8 and EdU assays; evaluating the effects of knocked down and overexpressed CEBPA on cell proliferation using Transwell experiments; examining the correlation of CEBPA with T cells and B cells using mIHC analysis.

Results Consensus clustering analysis identified three molecular subtypes, suggesting significant differential expression of these ARGs in NSCLC prognosis and clinical pathological parameters. There was significant differential expression between the two risk groups in the prognostic risk model, with $P < 0.001$. The risk score of the prognostic risk model was also $P < 0.001$. CEBPA exhibited higher mRNA and protein expression levels in NSCLC cell lines. Knockdown of CEBPA significantly reduced mRNA and protein expression levels of CEBPB, YWHAZ, ABL1, and CDK1 in H1650 and A549 cells. siRNA-mediated knockdown of CEBPA markedly inhibited proliferation, migration, and invasion of NSCLC cells, whereas overexpression of CEBPA showed the opposite trend. mIHC results indicated a significant increase in CD3 + CD4+, CD3 + CD8+, and CD20 + cell counts in the high CEBPA expression group.

†Jiaqi Zhu, Xiaoren Zhu and Conglin Shi have contributed equally to this work.

*Correspondence:
Yi Jin
jin_yibai@126.com
Tianyi Wang
13862965891@163.com
Jianle Chen
jsshcjl@163.com

Full list of author information is available at the end of the article

Conclusions The risk score of the prognostic risk model can serve as an independent prognostic factor, guiding the diagnosis and treatment of NSCLC. CEBPA may serve as a potential tumor biomarker and immune target, facilitating further exploration of the biological functions and immunological relevance in NSCLC.

Keywords Non-small cell lung cancer, Prognostic model, LASSO regression, Tumor immune microenvironment, Therapeutic target

Introduction

Lung cancer is the most common type of cancer and a leading cause of cancer-related deaths worldwide. The death toll has exceeded the sum of breast cancer, colorectal cancer and pancreatic cancer [1–4]. Non-small cell lung cancer (NSCLC) constitutes the majority of lung cancer cases [5]. Despite early detection and advances in multiple treatment modalities including surgery, radiotherapy, chemotherapy, and immunotherapy, its five-year overall survival rate remains below 20% [6]. Recent studies have revealed significant gene expression variations in the occurrence and progression of NSCLC, highlighting the need to identify stable and precise tumor biomarkers as well as novel therapeutic targets [7–9].

Aging, an inevitable and essential biological process, is characterized by the degeneration and loss of material structure composition and physiological function [10, 11]. It has been recognized as a critical risk factor in cancer development and progression. Aging-related genes (ARGs) have shown both inhibitory effects on cell growth to suppress cancer development and progression [12–15]. Moreover, aging has gained increasing attention in cancer research as it has been a tumor biomarker aiding in the diagnosis and prognosis of various cancers [16, 17]. CCAAT/Enhancer-Binding Protein Alpha (CEBPA), the main focus of this study, is a transcription factor that coordinates proliferation arrest and differentiation of myeloid progenitor cells, liver cells, and lung and placental cells [18–20]. However, the biological function of CEBPA in NSCLC remain poorly understood, and further investigation is required to establish its role as a tumor marker.

The tumor immune microenvironment (TIME) is critical in cancer development [21, 22]. TIME is closely related to tumor immunosuppression or activation. In addition to tumor cells, TIME also includes innate immune cells, adaptive immune cells, stromal cells, endothelial cells and fibroblasts [23]. T cells and B cells, being the most widely distributed lymphocyte populations, have a significant impact within the TIME [24]. It is noteworthy that many immune cells have dual roles in promoting and inhibiting tumor growth [25]. T cells, characterized by the expression of CD3, CD4, and CD8, are of particular importance in NSCLC development, while CD20 is a common B cell marker [26]. Identifying immune markers facilitates the discovery of potential immune targets, consequently advancing the field of immunotherapy [27].

In this study, we extensively reviewed the literature and selected 25 highly relevant ARGs from the Human Aging Gene Repository (HAGR) for analysis. The Cancer Genome Atlas database (TCGA) and Gene Expression Omnibus Database (GEO) were utilized in the analysis. Consensus clustering analysis was applied to identify molecular subtypes of ARGs in NSCLC patients, indicating that the selected ARGs have a substantial impact on NSCLC prognosis and clinicopathological parameters. Subsequently, a prognostic model was constructed using the screened genes to accurately evaluate the relevance and prognostic value of ARGs in NSCLC. Next, we constructed a nomogram to verify that the risk score could serve as an independent prognostic factor for NSCLC. Furthermore, the validation process was replicated in two GEO cohorts using the same algorithm, confirming the accuracy of the prognostic model.

The mRNA expression levels of seven prognostic risk genes in NSCLC cell lines were analyzed by qPCR method, and their correlations were further analyzed. After extensive literature review, CEBPA was finally selected as the best prognostic risk gene. Subsequent in vitro cell experiments, including qPCR, Western Blot, CCK-8, EdU, and Transwell experiments, further verified that knocking down CEBPA significantly inhibited the proliferation, migration, and invasion of NSCLC cells. Conversely, forced overexpression of CEBPA demonstrated pro-oncogenic effects in NSCLC cells. Then, we used ESTIMATE and ssGSEA algorithms to analyze the immune microenvironment and evaluated whether ARG can affect the occurrence and progression of NSCLC through the immune microenvironment pathway. Finally, we evaluated the colocalization of CEBPA with immune cell markers using multiplex immunohistochemistry (mIHC) technology on tissue microarrays. CEBPA can be used as a tumor marker to guide the diagnosis and immune-related research of NSCLC.

Materials and methods

Data sources

In the study, the relevant information of the databases can be found in Table S1.To ensure the accuracy of the study, data from NSCLC patients without survival information and clinicopathological parameters were removed from the analysis.

Selection of ARGs and PPI network analysis

25 highly suitable ARGs were obtained from the HAGR Genage database (Table S2). The STRING database is used to draw their protein-protein interaction (PPI), which is currently a relatively authoritative database for the study of protein interactions. Required score is set to medium confidence (0.400). Through this database, we can easily retrieve the interaction relationship between known proteins, which helps to better understand the complex regulatory network in organisms. Xiantao academic software was used for further visualization. PPI-related data are attached in Table S3.

Consensus clustering analysis and heatmaps

Consensus clustering analysis is a relatively common unsupervised classification method for cancer subtypes. We used the "Consensus clustering Plus" R package to classify samples into different molecular subtypes based on different mRNA expression levels. The color scale changes in the heatmap indicate the expression level. Purple indicates low values, and yellow indicates high values. A color block represents a numerical value. The yellower the color, the higher the expression level, and the purpler the color, the lower the expression level. Z-score normalization is performed on each gene (row) so that the mean of each row becomes 0 and the standard deviation becomes 1.

Construction and verification of prognostic risk model

Firstly, 15 ARGs with prognostic value were identified by least absolute shrinkage and selection operator(LASSO) regression, and the setting $P<0.05$ for screening. Cross-validation was used to select the optimal lambda parameter, using the criterion of minimizing the mean cross-validation error within one standard error of the minimum value (1-SE rule). The cross-validation method used ten-fold cross-validation to determine the lambda that minimized the prediction error. In addition, the prognostic value of ARGs was evaluated within the LASSO framework using the Cox proportional hazards regression model. Survival analysis was performed to evaluate the relationship between ARG expression levels and patient survival outcomes. The specific formula of the risk score is as follows:

$$\mathrm{RiskScore} = \mathrm{Exp}\ (\mathrm{ARG1}) \times \beta 1 + \mathrm{Exp}\ (\mathrm{ARG2}) \times \beta 2 + \ldots + \mathrm{Exp}\ (\mathrm{ARGn}) \times \beta \mathrm{n}$$

Exp represents the expression level of ARGs, and β represents the regression coefficient. The total sample size was then divided into two groups based on the cutoff. Receiver Operating Characteristic (ROC) analysis based on overall survival, risk score, and clinicopathological parameters was used to evaluate the accuracy of the model. Decision Curve Analysis (DCA) tested the performance of the model. In addition, 3D Principal Component Analysis (3DPCA) analysis proved that the seven genes had a good separation status in three different clusters and two different risk groups, which again verified the accuracy of the model. sex and stability.

Nomogram creation

Nomograms are a visualization tool that reduces predictive models to single numerical estimates of event probabilities on an individual patient basis [28]. We developed a nomogram utilizing three-year data on overall survival (OS), risk score, and clinicopathological parameters in patients with NSCLC. In addition, we generated calibration curves to assess the expected levels of nomograms.

Duplicate validation for two GEO external queues

We obtained two cohorts, GSE30219 and GSE68465, from the GEO database, and used the same formula to calculate the risk score for repeated validation. The optimal cutoff is used for grouping. Kaplan-Meier analysis and ROC were used to calculate OS and assess model accuracy, respectively.

Immune microenvironment analysis

In this study, the immune microenvironment analysis was conducted using the ESTIMATE and ssGSEA algorithms. The parameters for ESTIMATE were set according to the default guidelines provided by the ESTIMATE package, which is widely used in transcriptomic studies to predict the infiltration of stromal and immune cells in tumor samples.In ssGSEA, the parameters were set to normalize enrichment scores to facilitate comparison between samples. Specific gene sets, curated from publicly available immune cell markers databases, were employed to identify the various immune cell types. These gene sets include markers for T cells, B cells, macrophages, dendritic cells, and other immune cell subsets. The ssGSEA algorithm calculates an enrichment score for each gene set in each sample, which reflects the degree to which the genes in a particular set are coordinately up- or down-regulated within a sample.

Cells, cell culture and transfection

The Cell Bank of the Chinese Academy of Sciences provides human bronchial epithelial-like cell lines (16HBE) and human lung cancer cell lines (A549 and H1650). 16HBE was cultured in RPMI-1640 medium containing 10% fetal bovine serum (FBS), while A549 and H1650 were cultured in DMEM medium with 10% FBS. We knocked down CEBPA expression using two different classes of siRNA. 24 h after transfection, refresh the medium and incubate for 48 h in a suitable environment.

We proceeded to verify efficiency by qPCR and WB. The CP reagent, CEBPA siRNA (si-CEBPA#1#2) and nonspecific siRNA (NC) used to transfect cells were all from Ribobio (Guangzhou, China). The overexpression plasmid we used was from ORIGENE (Wuxi, China). The sequence data of CEBPA siRNA and overexpression plasmid are in Table S4.

Cell proliferation

The CCK-8 assay was employed to evaluate cell proliferation. A total of 2×10^3 cells per well were seeded into 96-well plates and cultured for a specific period. After transfection with siRNA under appropriate conditions, the cells were incubated for 0, 24, 48, and 72 h. Following the incubation, 10 μL of CCK-8 reagent (Biosharp, China) was added to each well according to the manufacturer's instructions. The cells were further incubated for 3 hours and the absorbance at 450 nm was measured using a microplate reader. This measurement provided an indication of cell proliferation levels. Additionally, the proliferation levels of A549 and H1650 cells were assessed using an EdU kit (Ribobio, China). The cells were seeded into 24-well tissue culture plates at a density of 5×10^4 cells per well. EdU (50 μM) was added to each well and incubated for 4 hours. Nuclei were then co-stained with DAPI and observed using fluorescence microscopy. The ratio of cell proliferation was determined by assessing the fluorescence intensity of EdU-positive cells.

Cell migration and invasion

To evaluate the migration and invasion abilities of NSCLC cell lines with knockdown and overexpression CEBPA, the researchers used Transwell chambers from (BIOFIL, China). For migration assays without Matrigel coating, 5×10^4 cells in 200 μL of serum-free DMEM were added to each upper chamber of the Transwell. The lower chamber was filled with 600 μL of DMEM containing 20% FBS. This setup was then incubated overnight at 37 °C with 5% CO^2 conditions. After incubation, cells that migrated to the bottom of the membrane were fixed with 4% paraformaldehyde for 20 min. Subsequently, they were stained with 2.5% crystal violet 24 h later. Three fields of view were analyzed per sample, and cell counts were performed using ImageJ software. For invasion assays, Transwell chambers with pre-coated upper chambers of 250 μg/mL Matrigel were used. The subsequent steps of the invasion assay were the same as the migration assay described above.

qPCR

Total RNA was isolated from cells using Invitrogen Trizol reagent (Servicebio, China). The RNA was then reverse transcribed into cDNA using the QuantiTect Reverse Transcription Kit. qPCR was performed by SYBR Green PCR kit (Ribobio, Guangzhou) and QuantStudio 5 real-time PCR system. The 2-ΔΔCt method was used for normalized quantification. Gene primer sequences are shown in Table S5.

Western blotting

Total protein was extracted with protein lysis buffer, and protein concentration was measured. Protein samples were analyzed using 10% SDS-PAGE and electrophoretically transferred to PVDF membranes (Millipore, Bedford, MA, USA). Following transfer, they were blocked with 10% skimmed milk powder from BD (USA) at an appropriate temperature for 1 h to prevent nonspecific binding. Subsequently, the membranes were incubated with diluted primary antibodies at 4 °C overnight. Following the primary antibody incubation, the membranes were washed to remove any unbound antibody and then exposed to an HRP-conjugated secondary antibody for 1 h at room temperature. ImageJ was used for data quantification.

Human tissue sample collection

The tissue microarray (TMA) used in this study included 195 NSCLC specimen tissues, and each sample tissue was averaged into a dot array with a diameter of 2 mm on a TMA slide. Patient specimens were obtained from September 2015 to September 2022 by the Department of Pathology, Affiliated Hospital of Nantong University. The patients had not undergone any treatment such as radiotherapy, chemotherapy and immunotherapy before surgery.

Multiplex immunohistochemistry (mIHC)

To analyze NSCLC TMA slides, the Opal 7-color manual IHC kit from (PerkinElmer, USA) was used for staining. The optimal concentration and conditions for each antibody were determined to establish an optimal staining protocol.The TMA slides were baked in an oven at 70 °C for 2 h. Deparaffinization was performed using xylene, followed by hydration with ethanol. Subsequently, the slides were fixed with 10% formalin for 10 min. The TMA slides were placed in AR6 buffer and AR9 buffer (AKOYA, USA) by microwave heating for antigen retrieval, and blocked with blocking solution (AKOYA, USA) for 10 min. Primary antibodies were incubated overnight at 4 °C. The next day, slides were incubated at room temperature for 30 min and incubated with secondary antibody Opal™ polymer HRP Ms+Rb (Perkin Elmer, USA) for 10 min. DAPI was used to stain nuclei and seal slides. We analyzed and imaged using Vectra 3.0 and scored using inForm® cell analysis software.

The antibodies involved are as follows: Rabbit anti-CD3 (CST, USA), Rabbit anti-CD4 (Abcam, England), Rabbit anti-CD8 (Abcam, England), Rabbit anti-CD20(Abcam,

England), Rabbit anti-CEBPA (CST, USA), Anti-mouse cytokeratin (Biobyt, England) and DAPI (Sigma, USA).

Statistical analysis

All statistical analyzes were done using R (version 4.0.4), GraphPad Prism 8.0, and Xiantao academic software.

Results

Differential expression and consensus clustering analysis of ARGs

In this study, the researchers aimed to identify 25 ARGs suitable for their investigation. These ARGs were selected from the HAGR database based on previous studies and relevant literature reports. First, we evaluated the degree of association of these ARGs in the STRING database, and used Xiantao academic analysis software to construct a mutual aid network diagram for visualization, and found that 21 ARGs exhibited a high level of association (Fig. 1A). Additionally, we analyzed the correlation between these ARGs using a diagonal correlation heatmap (Fig. 1B). The heatmap indicated a significant correlation among the ARGs. To further investigate the expression levels of the selected ARGs, we utilized data from the TCGA database. A heatmap was used to assess the expression levels of ARGs in different samples. The results showed that the expression levels of most ARGs varied significantly (Fig. 1C).

To explore the modification pattern and molecular subtype relationship of the selected ARGs in NSCLC, the researchers combined data from the TCGA-NSCLC data source and the GSE50081 dataset. These datasets were subjected to unsupervised Consensus clustering analysis. The CDF value was used to determine the optimal number of clusters, which was found to be 3 (K=3). Consequently, the total sample was divided into three clusters (Fig. 1E). Among them, there were 434 cases in cluster A, accounting for about 36.8%, 420 cases in cluster B, accounting for 35.6%, and 326 cases in cluster C, accounting for about 27.6%. Kaplan-Meier survival curve analysis showed that patients in cluster C had the highest overall survival rate and the best survival prognostic value, while patients in cluster A had the lowest overall

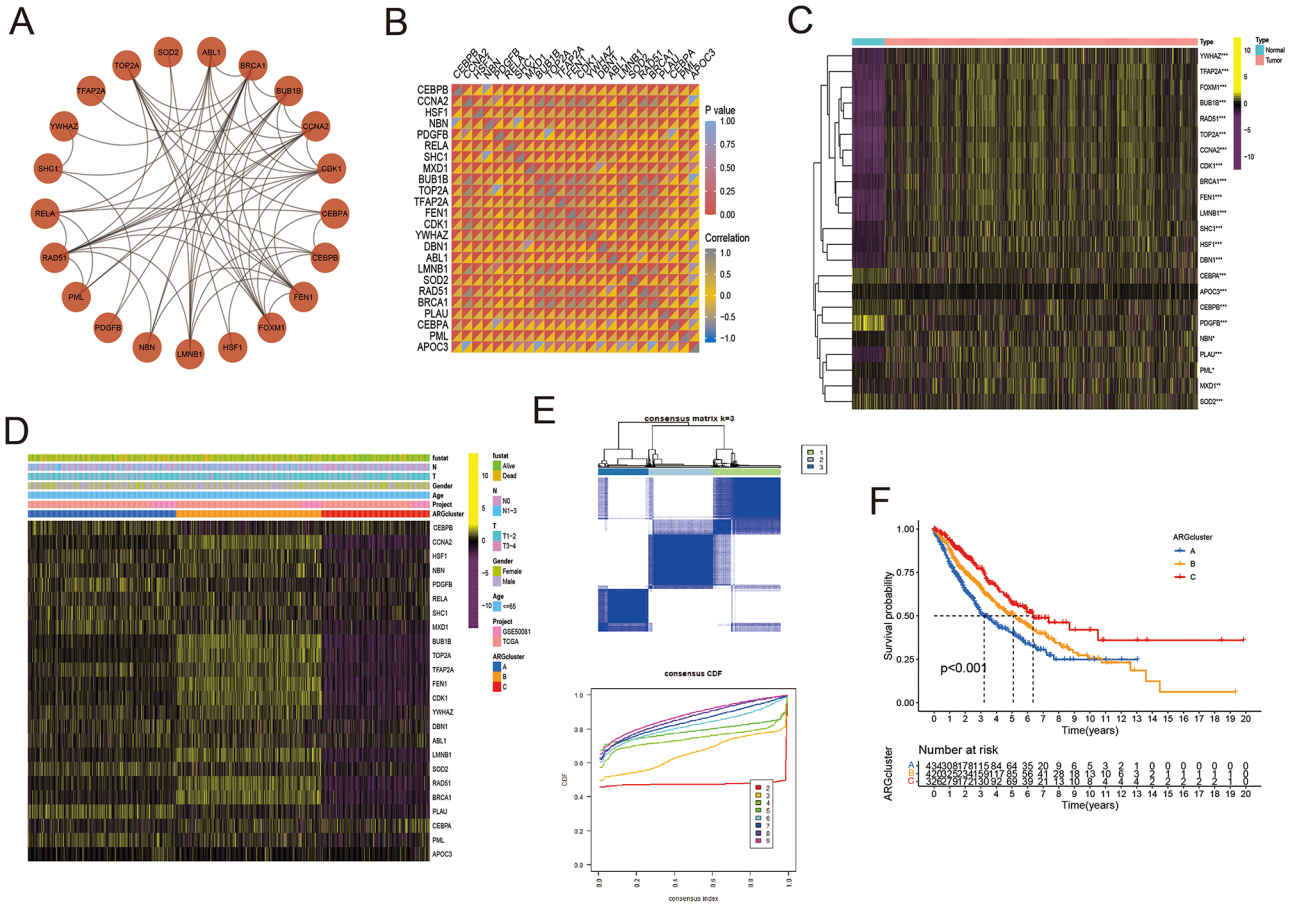

Fig. 1 Differential Expression and Consensus Clustering Analysis of ARGs (**A**) PPI plot of ARGs. (**B**) Diagonal correlation plot of interactions. (**C**) Heatmap showing ARGs expression levels in two different tissues. (**D**) Heatmap showing the correlation of subtypes in different clinicopathological parameters. (**E**) Optimal matrix type k=3 and CDF curves for consensus cluster analysis. (**F**) Survival analysis plots of the three subtypes of all NSCLC patients (*$P<0.05$; **$P<0.01$; ***$P<0.001$)

survival rate and the worst prognosis(Fig. 1F). Furthermore, we analyzed the expression levels of molecular subtypes in relation to clinicopathological parameters such as age, sex, and TMN stage. Heatmaps were generated to visualize the differences in expression levels (Fig. 1D), and significant distinctions were observed. In summary, this study, based on 25 highly relevant ARGs, uses consensus clustering analysis to preliminarily determine that the expression levels of the selected ARGs show significant differences. This analysis effectively identifies good molecular subtypes, demonstrating significant evaluative value in prognosis and clinical pathological parameters. It indicates that these ARGs play an important role in the occurrence and progression of NSCLC. Further research is needed to analyze their potential biological functions and molecular mechanisms.

Identification of prognostic risk model

To better evaluate the prognostic value of ARGs in NSCLC, an ARGs-based prognostic risk model was constructed. Initially, 1000 repeated iterations of LASSO regression analysis were conducted to determine the optimal lambda parameters for the model. As a result, 15 ARGs were selected as potential candidates (Fig. 2A-B). Subsequently, multivariate COX analysis was performed, and finally 7 genes were retained to construct the prognostic risk model. Then, all NSCLC cohorts were divided into two risk groups, high and low, using the median value as the cutoff. Kaplan-Meier analysis shows that the

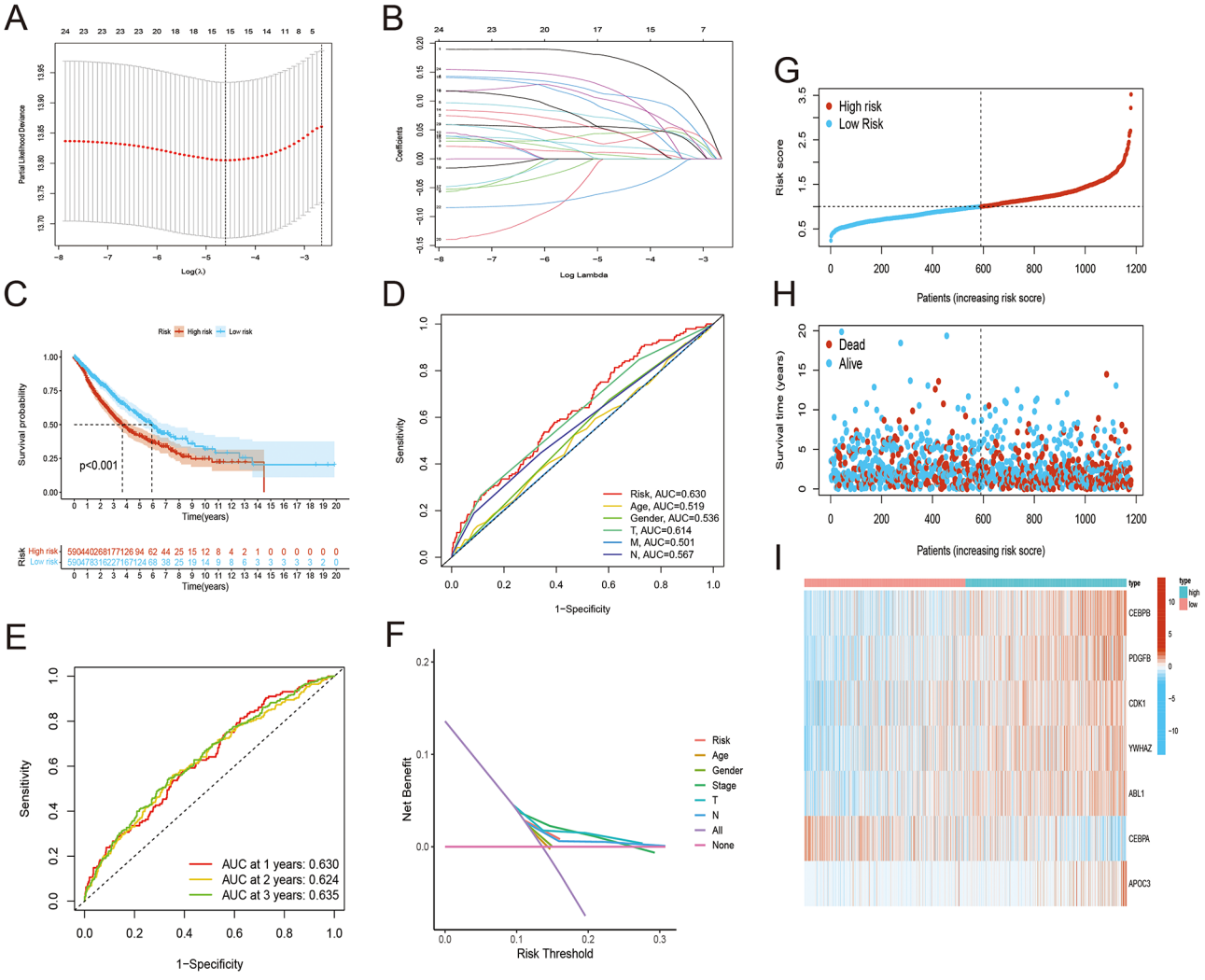

Fig. 2 Identification of Prognostic Risk Model (**A**) Based on the lowest standard of OS value, lambda was screened through 20 times of cross-validation in LASSO analysis. (**B**) Coefficient profile: cavity curve. (**C**) Survival curve analysis for the two risk groups. (**D**) ROC curves showing the survival rate at different times for the prognostic risk model. (**E**) ROC curves evaluating the combined prognostic value of different clinicopathological parameters and prognostic risk models. (**F**) DCA analysis demonstrating the net benefit between the prognostic risk model and clinicopathological parameters. (**G**-**I**) Risk score curves, patient survival status, and heatmaps of expression of seven risk-prognostic genes

overall survival rate of patients in the high-risk group is lower and the survival prognosis is worse (Fig. 2C). Time-dependent ROC analysis showed that the area under the curve (AUC) at 3 years were 0.630, 0.624 and 0.635, indicating the prognostic risk model has good stability (Fig. 2E). Figure 2G-I shows the risk score curve, the patient's survival status and the heat map of the expression levels of 7 prognostic risk genes. Moreover, we compared the differences in clinical parameters between the two risk groups. We initially drew the clinical variable correlation ROC diagram and DCA diagram, the results showed that the two risk groups differed significantly in terms of age, sex and TMN stage (Fig. 2D, F).

Correlation analysis of clinicopathological parameters of ARGs

To further assess the value of the model in relation to clinicopathological parameters, several analyses were conducted. Initially, Sankey diagrams were generated to illustrate the associations between the two risk groups, three different cluster classes, survival status, and stage (Figure S1A). The proportions of clinical variables in the two risk groups were calculated and analyzed. It was found that various clinicopathological parameters exhibited significant differences between the two risk groups in the total NSCLC cohort (Figure S1D-F). In addition, a heatmap showing the association between risk scores of prognostic risk genes and NSCLC-related clinicopathological variables was found to be significantly different (Figure S1G). Finally, a 3D Principal Component Analysis (PCA) plot was constructed. This plot demonstrated that the seven risk prognostic genes were well separated within the three different clusters and the two different risk groups, thereby reinforcing the accuracy of the model (Figure S1B-C). In summary, the prognostic risk model we constructed not only has good stability and accuracy, but also can guide the survival prognosis of different clinicopathological parameters.

Independent prognostic factors and nomogram

First, univariate and multivariate COX analysis was used to validate the predictive ability of the model and to verify whether the risk score was an independent prognostic factor for NSCLC. In univariate COX analysis, riskscore: hazard ratio (HR): 2.254, 95CI%: 1.795–2.83, $P<0.001$. In multivariate COX analysis, riskscore: HR: 2.047, 95CI%: 1.624–2.581, $P<0.001$(Fig. 3A). These results strengthen the role of the Riskscore as an independent predictor of prognosis in NSCLC. In order to develop a visual prognostic model, a nomogram was constructed. This nomogram combines a risk score with clinical parameters such as age, sex, and TMN stage. Effective prediction of three-year overall survival in NSCLC patients (Fig. 3B). In addition, the calibration curve showed that the predicted curve was close to the standard curve, which effectively verified that the predicted survival rate was consistent with the actual survival situation (Fig. 3C-E). These results suggest that the risk score can be used as an independent prognostic factor, and the construction of the nomogram has a predictive advantage.

Duplicate validation in GEO queues

To further explore the stability and effectiveness of the prognostic risk model, the risk score was tested in the GSE30219 and GSE68465 cohorts through the same analysis process. The optimal cut-off value was defined as the critical value, and the patients were divided into high-risk group and low-risk group. As expected, the prognostic OS of the low-risk group was significantly better than that of the high-risk group (Figure S2A, E). Figures S2B-C and F-G show the risk score distribution and survival status, respectively. Furthermore, ROC analysis was performed to evaluate the predictive performance of the prognostic risk model. In GSE30219, the AUC values at 3 years were calculated as 0.688, 0.691, and 0.679, respectively (Figure S2D). In GSE68465, the AUC values at 1 year, 2 years, and 3 years were calculated as 0.683, 0.640, and 0.628, respectively (Figure S2H). This shows that the prognostic risk model can be used to predict the prognosis of NSCLC and has good value and significance.

Identification of prognostic risk genes

Univariate and multivariate COX analysis evaluated seven prognostic risk genes, including ABL Proto-Oncogene 1 (ABL1), Apolipoprotein C3 (APOC3), Cyclin-dependent kinase 1 (CDK1), Tyrosine 3-Monooxygenase/Tryptophan 5-Monooxygenase Activation Protein Zeta (YWHAZ), CCAAT enhancer Binding protein Beta (CEBPB), Platelet Derived Growth Factor Subunit B (PDGFB) and CEBPA. In the TCGA database, there is a general correlation between these prognostic risk genes (Fig. 4A). To analyze mRNA expression in NSCLC, we performed qPCR in a human bronchial epithelial-like cell line (16HBE) and two lung cancer cell lines (A549, H1650) and found that most of the prognostic risk genes were significantly different and in the lung cancer cell lines Significantly high expression (Fig. 4B). Notably, ABL1 and CEBPA exhibited the most significant differences in expression levels. Extensive literature research has been conducted, and the molecular mechanisms of ABL1 have been thoroughly studied in various cancer types [29–32]. On the other hand, CEBPA acts as a protein-coding gene, which plays an important role in cancers such as acute myeloid leukemia, liver cancer and ovarian cancer [33–35]. However, there are relatively few reports on the involvement of CEBPA in lung cancer. Therefore, it was chosen as the main research focus of this study to conduct further in-depth research.

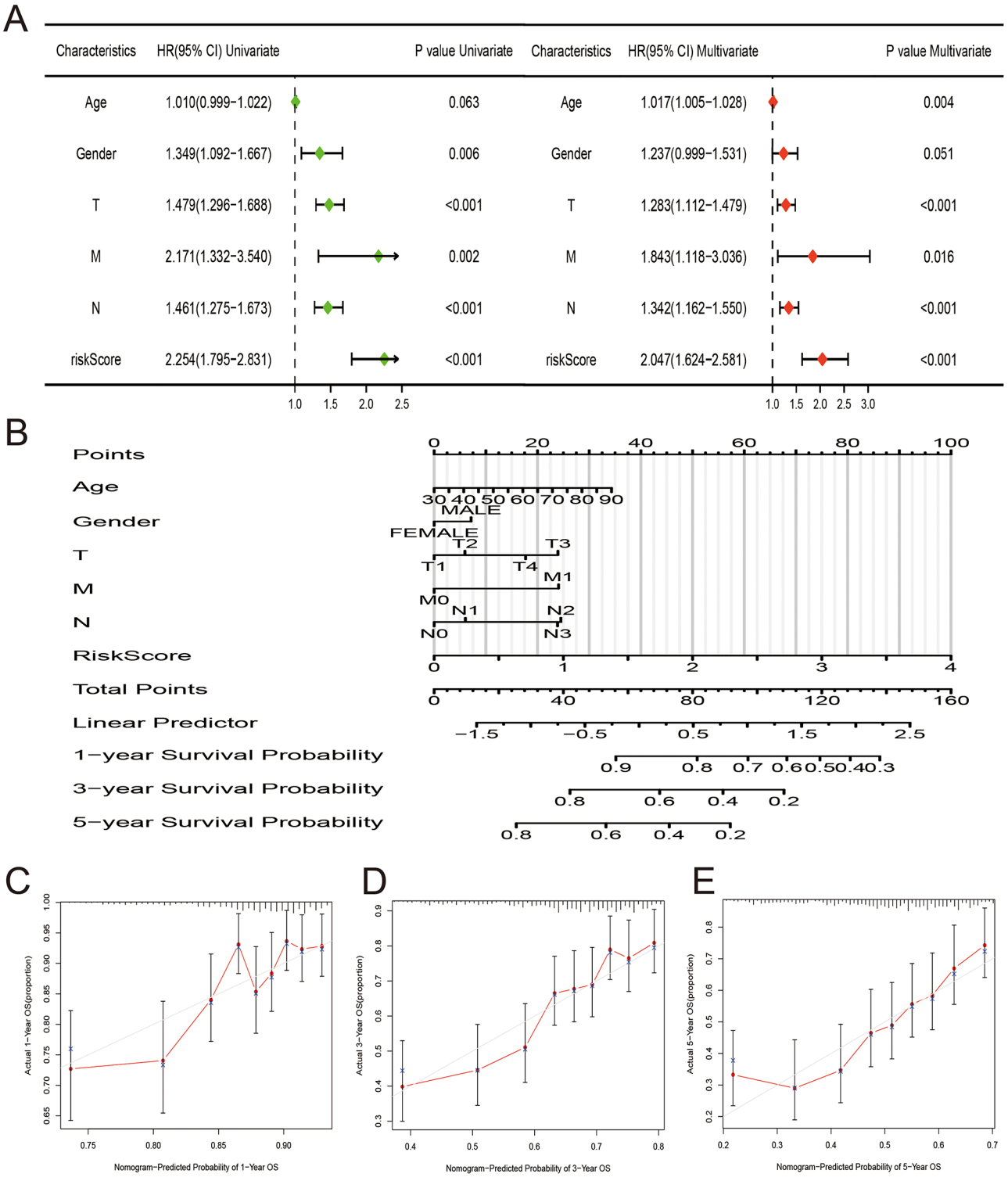

Fig. 3 Independent Prognostic Factors and Nomogram (**A**) Evaluation of clinicopathological parameters and risk scores by univariate COX analysis and multivariate COX analysis. (**B**) Nomogram constructed based on risk score and clinicopathological parameters (Age, Gender, T, M, N). (**C**-**E**) Calibration curves for nomogram predictions

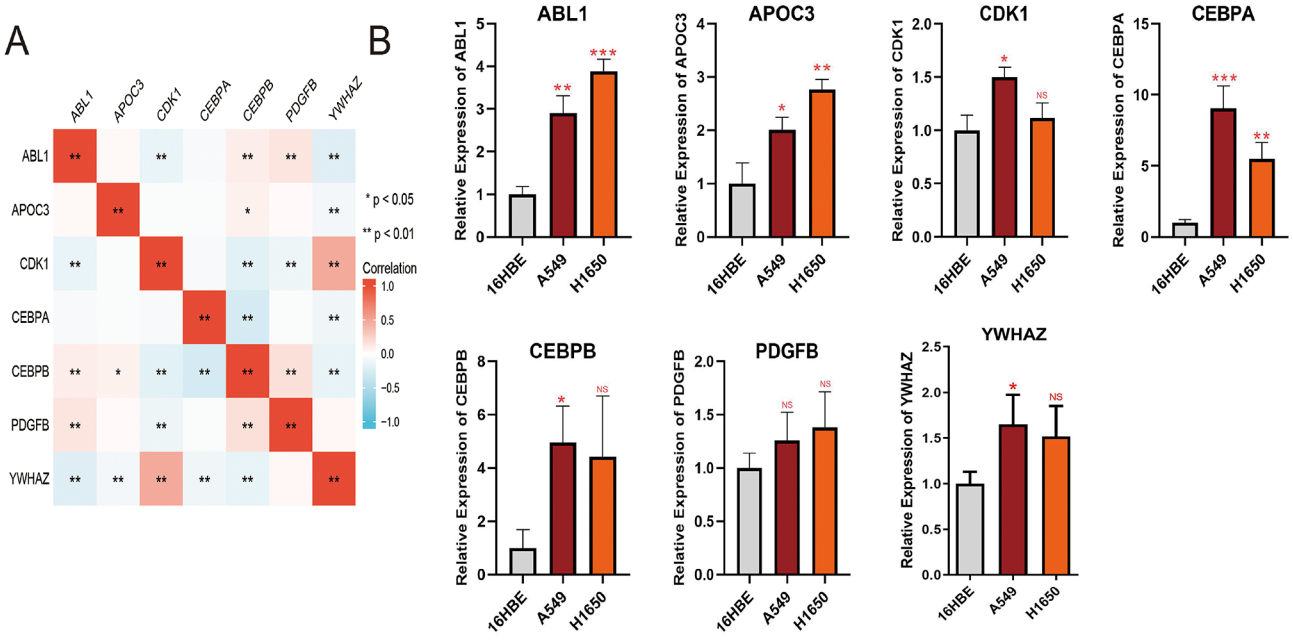

Fig. 4 Identification of Prognostic Risk Genes (**A**) Spearman correlation analysis among the 7 best prognostic genes in TCGA-NSCLC. (**B**) mRNA levels quantified using qPCR analysis in human bronchial epithelioid cells and two NSCLC cell lines (*$p < 0.05$, **$p < 0.01$, ***$p < 0.001$)

Interactions between prognostic risk genes

To further understand the interactions between these genes, we analyzed the expression levels of the other six markers when CEBPA was knocked down based on H1650 and A549 cells. PCR results showed that siRNA knockdown of CEBPA significantly reduced the mRNA levels of CEBPB, YWHAZ, ABL1 and CDK1 in H1650 and A549 cells, but there was no significant difference in the expression changes of APCO3 and PDGFB (Fig. 5A-F). Western Bolt results can also support this trend. CEBPA knockout significantly reduced the protein expression levels of CEBPB, YWHAZ, ABL1 and CDK1 (Fig. 5G, H). PPI analysis network showed correlation with CEBPA, CEBPB, YWHAZ, ABL1 and CDK1 (Fig. 5I). Studies have shown that CEBPA and CEBPB are members of the C/EBP family, have similar DNA binding domains, and play regulatory roles in cell proliferation and differentiation [36]. T. Pabst et al. found that CEBPA mutations or silencing can synergize with BCR-ABL1 fusion to exacerbate leukemia development. Both genes are essential in the regulation of hematopoietic cells, and their dysregulation can significantly affect cancer progression [37]. ABL1 can influence the activity of CDK1 either directly or through upstream signaling pathways, thereby affecting cell cycle progression and cancer cell proliferation [38].

Influence of CEBPA on cell proliferation, migration and invasion

To explore the biological function of CEBPA in NSCLC cell lines, CEBPA siRNA was transduced into A549 and H1650 cells. This siRNA knockdown of CEBPA resulted in a significant decrease in mRNA and protein expression levels in NSCLC, as confirmed by qPCR and Western blot analysis. In H1650, the protein expression level decreased by about 30–40% after knocking down CEBPA, while in A549, the protein expression level decreased by about 20–30% after knocking down CEBPA (Fig. 6A-B). The CCK-8 assay was performed to assess the proliferation activity of H1650 and A549 cells with CEBPA knockdown. The results demonstrated that knockdown of CEBPA led to a significant decrease in the proliferation activity of both cell lines (Fig. 6C). To further evaluate the impact of CEBPA knockdown on cell proliferation, an EdU assay was conducted. The knockdown of CEBPA resulted in a reduced ratio of EdU-positive nuclei, indicating suppressed proliferation of H1650 and A549 cells (Fig. 6D). Transwell assays revealed that the migration of NSCLC cells was weakened. Matrigel Transwell assay showed that NSCLC cell invasion was also significantly reduced (Fig. 6E-F). In conclusion, siRNA knockdown of CEBPA can significantly inhibit the proliferation, migration and invasion of NSCLC cells.

Next, plasmids encoding CEBPA cDNA ("OE-CEBPA") were transduced into H1650 and A549 cells. Stable cell lines were established through selection with puromycin. Compared to control cells with the empty vector ("Vec"), the levels of CEBPA mRNA in OE-CEBPA cells were significantly increased (Fig. 7A), and protein expression levels were similarly upregulated (Fig. 7B). CCK-8 assay results showed that overexpression of CEBPA led to a significant increase in the proliferation of H1650

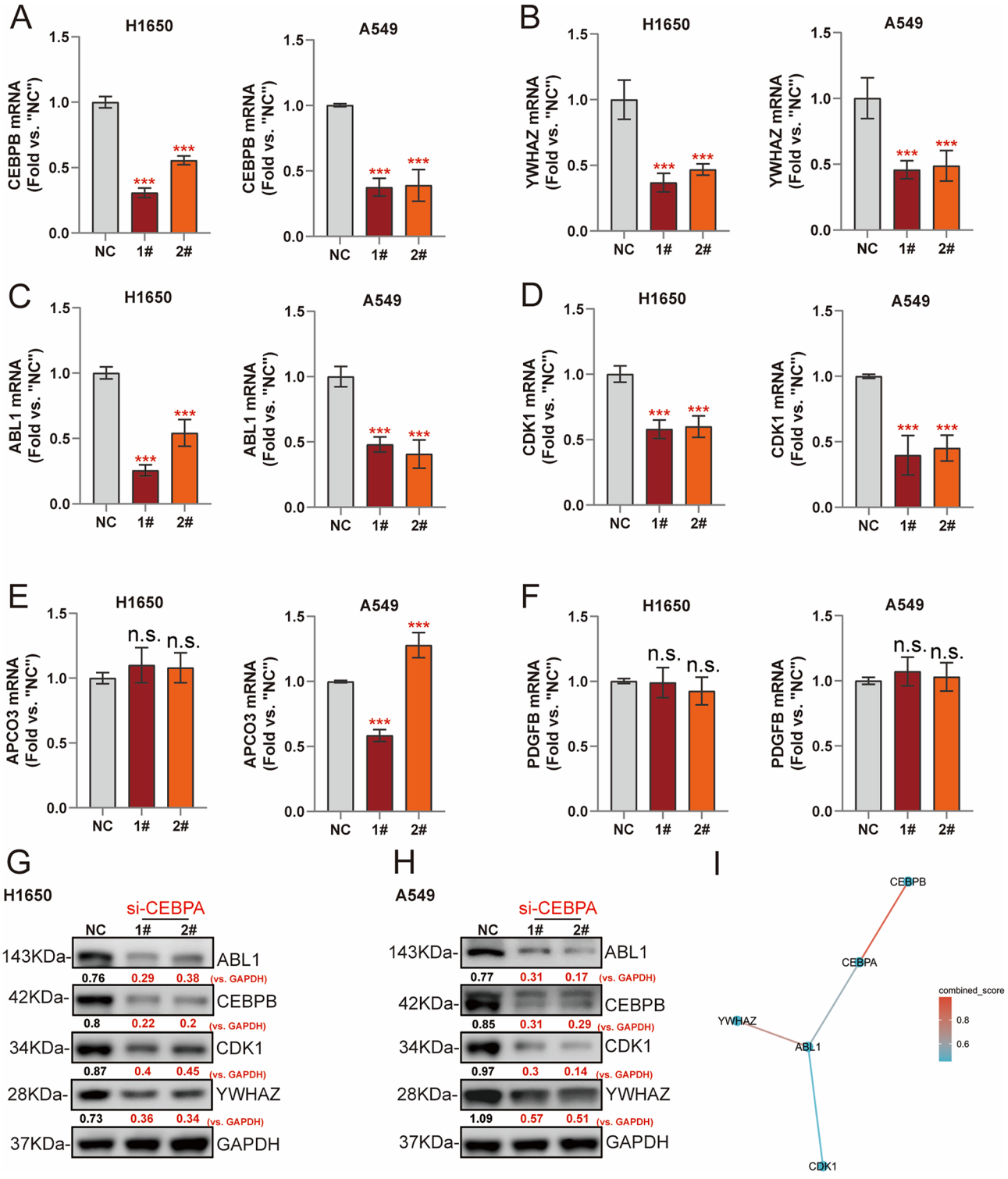

Fig. 5 Interactions between Prognostic Risk Genes (**A**-**F**) qPCR was used to evaluate the mRNA levels of CEBPB, YWHAZ, ABL1, CDK1, APCO3, and PDGFB in H1650 and A549 cells after siRNA knockdown of CEBPA. (**G**, **H**) Western Blot was used to evaluate the protein expression levels of CEBPB, YWHAZ, ABL1 and CDK1 in H1650 and A549 cells after siRNA knockdown of CEBPA. (**I**) PPI analysis of the correlation of prognostic risk genes. Error bars stand for mean ± standard deviation (SD, $n = 5$)

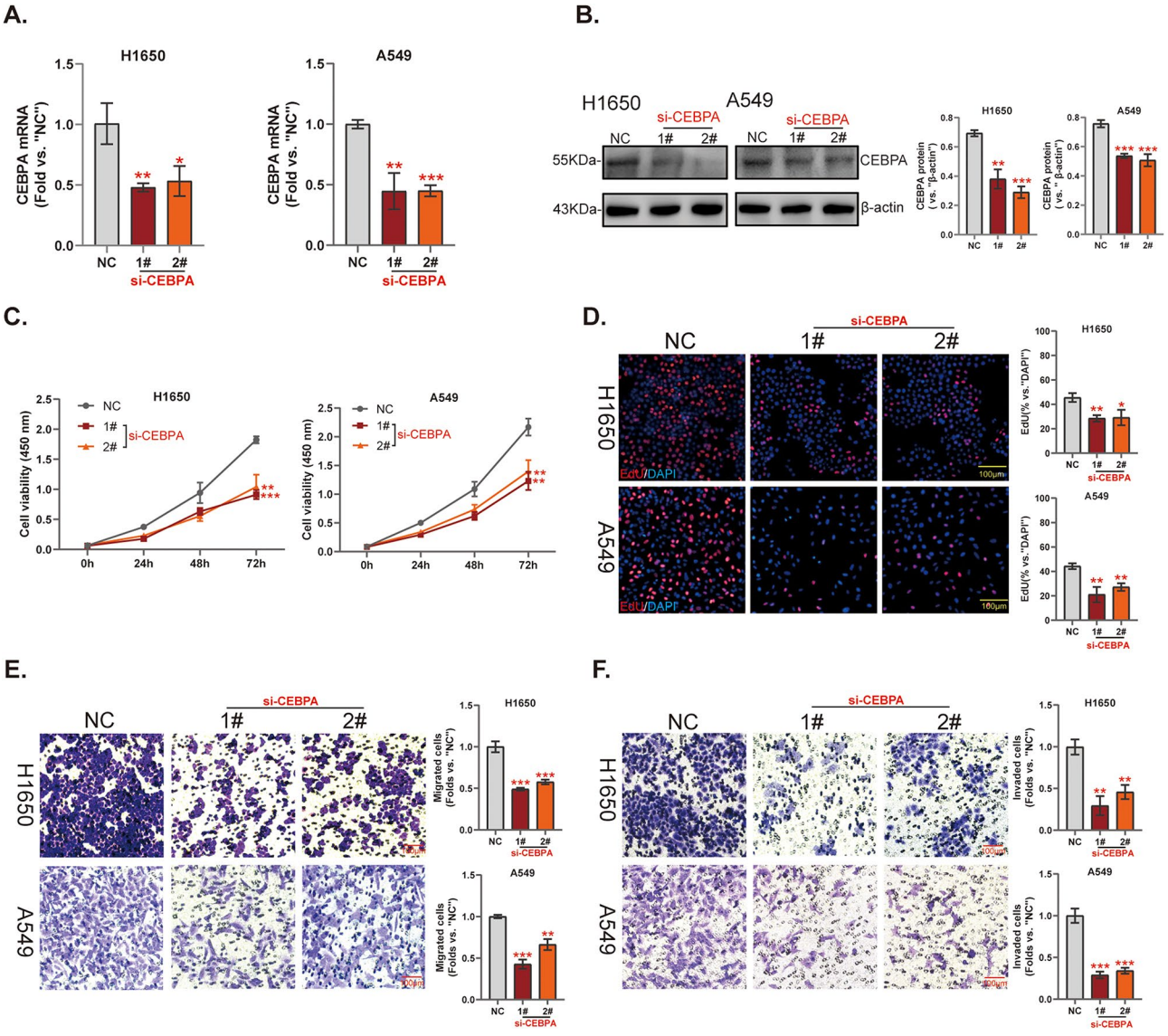

Fig. 6 Influence of CEBPA on Cell Proliferation, Migration and Invasion (**A**) and Western blot (**B**) were used to evaluate mRNA and protein expression levels after si-CEBPA transfection. CCK-8 (**C**) and EdU assays (**D**) were used to assess the proliferation capacity of H1650 and A549 cells. Cell migration and invasion abilities were measured by Transwell (**E**) and Matrigel Transwell assay (**F**) (*$p < 0.05$, **$p < 0.01$, ***$p < 0.001$). Human NSCLC cell lines (H1650 and A549) and si-CEBPA ("#1" and "#2") are suitable for (**A**-**F**)

and A549 cells (Fig. 7C). Functional studies indicated that the proportion of EdU-positive nuclei in OE-CEBPA H1650 and A549 cells was significantly higher, suggesting that CEBPA overexpression promoted cell proliferation (Fig. 7D). Additionally, CEBPA overexpression accelerated the invasion of H1650 and A549 cells (Fig. 7E).

Influence of CEBPA expression on immune microenvironment

To assess the influence of CEBPA expression on the immune microenvironment of NSCLC, we utilized the ESTIMATE algorithm to calculate matrix scores, immune scores, and ESTIMATE scores for patients in the two different risk groups. We observed significant differences only in the immune scores (Fig. 8A). Next, we analyzed the relationship between the immune infiltration levels of various immune cells, including T cells, B cells, NK cells, DC cells, mast cells, and neutrophils, and the expression of CEBPA. We found that high levels of CEBPA are associated with high infiltration of most immune cells but not with Th2 cells. We speculate that CEBPA might influence the activity or infiltration of Th2 cells through specific mechanisms: CEBPA may regulate the cytokine network to inhibit the differentiation or function of Th2 cells, leading to lower infiltration levels of Th2 cells compared to other immune cells. Additionally, CEBPA might activate certain immune evasion mechanisms specifically targeting Th2 cells, preventing them

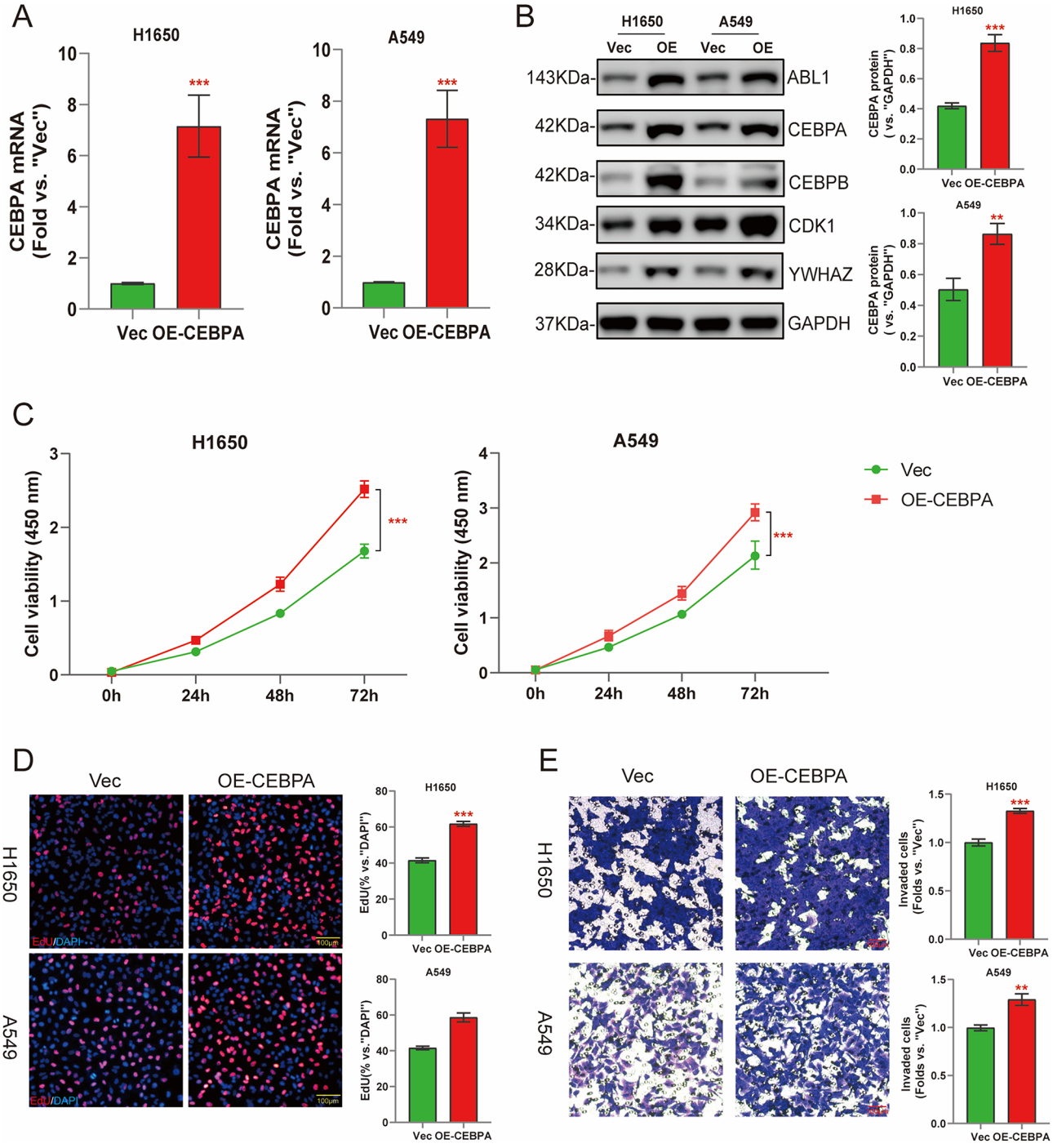

Fig. 7 Influence of CEBPA on Cell Proliferation, Migration and Invasion qPCR (**A**) and Western blot (**B**) were used to evaluate mRNA and protein expression level. CCK-8 (**C**) and EdU assays (**D**) were used to assess the proliferation capacity of H1650 and A549 cells. (**E**) Cell migration and invasion abilities were measured by Matrigel Transwell assay (*$p < 0.05$, **$p < 0.01$, ***$p < 0.001$)

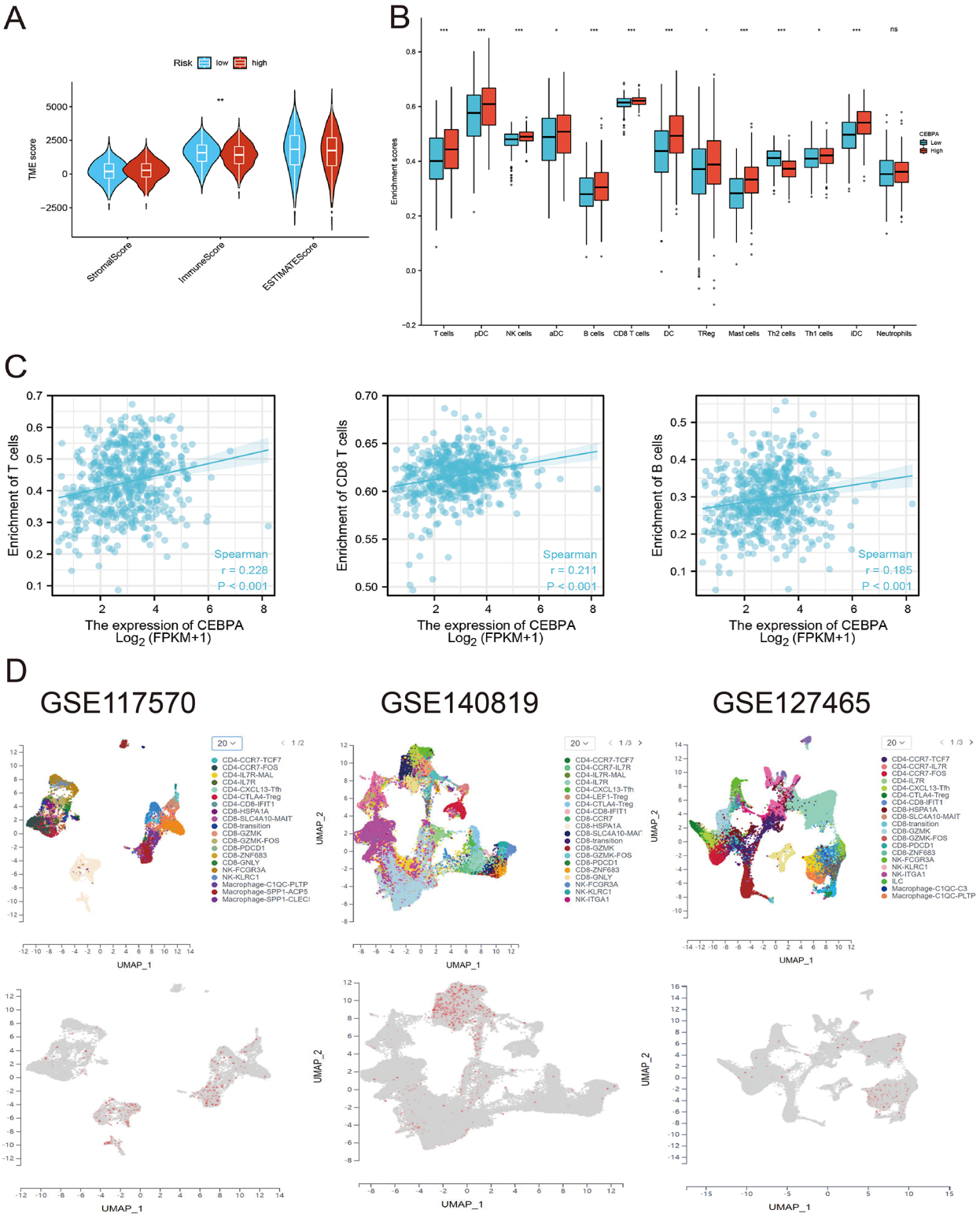

Fig. 8 Influence of CEBPA Expression on Immune Microenvironment (**A**) TME scores of two risk groups, including Stromal score, Immune score and Estimates score. (**B**) Levels of immune infiltration in T cells, B cells, NK cells, DC cells, mast cells, and neutrophils in the CEBPA high- and low-expression groups in the TCGA-NSCLC cohort. (**C**) Scatterplot showing the association of CEBPA with T cells, CD8 + T cells, and B cells. (**D**) Cell type cluster analysis

from effectively infiltrating the tumor region (Fig. 8B). To further explore the correlation between CEBPA expression and T cell and B cell infiltration levels, Spearman correlation analysis was performed. Scatter plots revealed positive correlations between CEBPA expression and infiltration levels of T cells and B cells, with a p-value less than 0.001 (Fig. 8C). Single cell data analysis showed that CEBPA was enriched in cells such as CD4, CD8, NK cells and macrophages(Fig. 8D).These findings indicate a significant immune correlation between CEBPA expression and T cells as well as B cells in NSCLC.

High expression of CEBPA in NSCLC recruit more immune cells

To investigate the protein expression levels and immune infiltration of CEBPA and four immune cell types (T cells: CD3, CD4, CD8, and B cells: CD20) in NSCLC, we conducted mIHC assays on TMA slides. The TMA slides allowed for simultaneous visualization of CD3, CD4, CD8, CD20, CEBPA, CK, and DAPI. By utilizing computational imaging, we examined the immune cell infiltration levels and protein expression patterns in NSCLC samples. The results revealed varying levels of immune cell infiltration among almost all NSCLC samples. Based on the median number of positive expressing cells, we divided the samples into two different expression groups for CEBPA and the immune cell markers. Analysis of the TMA slides demonstrated extensive infiltration of CD3+CD4+, CD3+CD8+, and CD20+cells in the immune microenvironment of NSCLC (Fig. 9A-B). Importantly, the high-expression group of CEBPA exhibited significantly increased numbers of CD3+CD4+, CD3+CD8+, and CD20+cells compared to the low-expression group (Fig. 9C). These results confirm the bioinformatics analysis and provide experimental verification that CEBPA is significantly correlated with increased infiltration of CD3+CD4+, CD3+CD8+, and CD20+cells in the tumor microenvironment of NSCLC.

Discussion

In recent times, the incidence and mortality rates of NSCLC have been steadily rising [39]. Despite significant advancements in cancer prevention, early screening, and surgical intervention for NSCLC, the prognosis remains poor [40, 41]. Therefore, there is an urgent need to mine novel tumor biomarkers and immunotherapy targets to improve the prognosis and survival of NSCLC patients [42, 43].

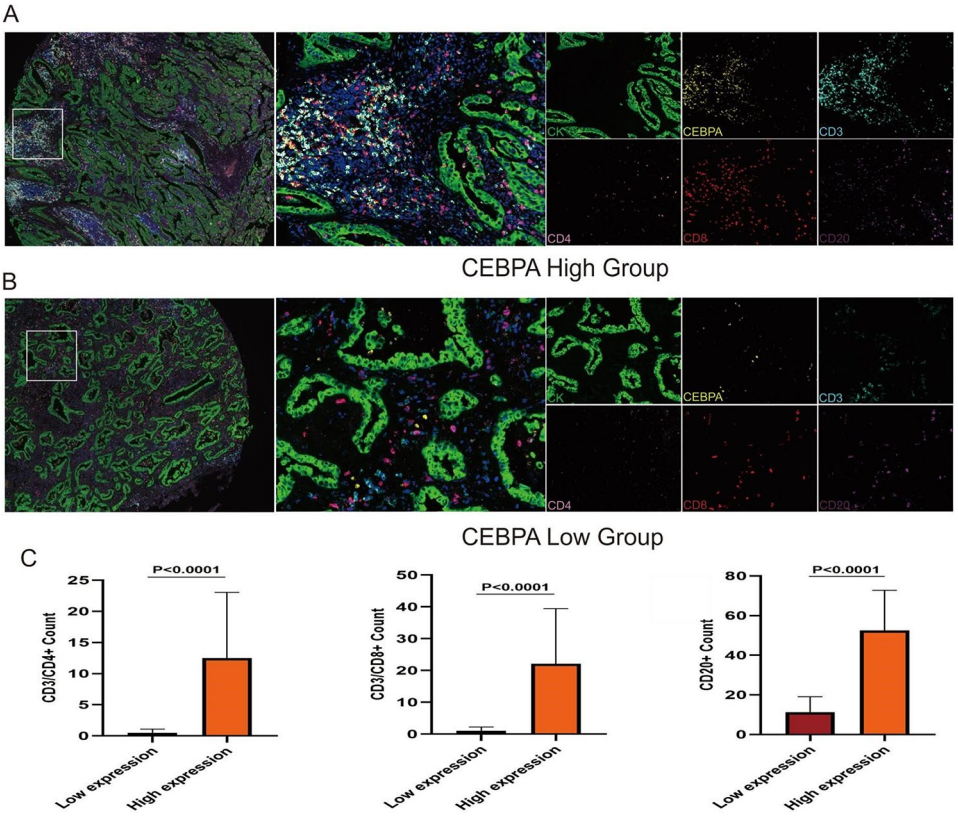

Fig. 9 High Expression of CEBPA in NSCLC Recruit More Immune Cells (**A**-**B**) Significantly representative multiplex immunohistochemical images for CEBPA, CD3, CD4, CD8, and CD20 in TMA of NSCLC. (**C**) Abundance of CD3+CD4+cells, CD3+CD8+cells, and CD20+immune infiltrates in NSCLC patients with high or low CEBPA expression

Studies have consistently demonstrated the strong association between aging and cancer, with a higher incidence of cancer occurring in the elderly population compared to younger individuals [44]. Aging has been identified as a major risk factor for tumors, including NSCLC. It actively participates in various biological processes that promote the development and progression of NSCLC [45, 46], and is significantly related to its poor prognosis [47]. Aging is a universal biological process observed in nearly all living organisms. In contrast, cancer is characterized by uncontrolled cell growth, resistance to apoptosis, distant metastasis, and the acquisition of new abnormal functions [48]. Aging is marked by the accumulation of cellular damage, leading to DNA damage, diminished tissue metabolism, and loss of organ function [49, 50]. These characteristics of aging stand in stark contrast to those of cancer. Multiple factors contribute to the association between aging and cancer development. Endogenous factors such as genetic factors, immunodeficiency, and endocrine factors, as well as exogenous factors including alcohol consumption, radiation exposure, and a high-calorie, high-fat diet, can induce oxidative stress and DNA damage. Inflammatory mediators secreted during aging, such as interleukins and monocyte chemoattractant proteins, create a conducive environment for carcinogenesis [51]. Simone et al. found that senescent cells typically exhibit elevated levels of reactive oxygen species (ROS), leading to oxidative stress. ROS can cause significant damage to cellular components, including DNA, proteins, and lipids, thereby promoting carcinogenesis. Oxidative stress is a known factor in the pathophysiology of NSCLC [52]. Dunyaporn et al. discovered that utilizing antioxidants or drugs that modulate ROS levels can mitigate oxidative stress, potentially reducing DNA damage and subsequent cancer risk [53]. Furthermore, related research indicates that immunosenescence leads to a decline in the production and function of immune cells such as T cells and B cells, reducing the body's ability to effectively detect and eliminate cancer cells [54]. Charlene et al. found that immunotherapies have shown promise in reinvigorating the aging immune system to effectively target cancer cells. Combining these with agents that modulate the immune response could enhance their efficacy in elderly NSCLC patients [55]. Therefore, it is of great significance to further study the connection between aging and the biological processes and treatment strategies of NSCLC development.

In this study, the comprehensive approach included bioinformatics analysis, in vitro cell function experiments, and immune-related studies. Initially, the expression levels of 25 ARGs in NSCLC samples and normal samples were analyzed using data from the TCGA database. The majority of the ARGs showed significant differential expression, indicating their suitability for this study and enabling systematic research. Subsequently, a combined cohort of patient samples from the TCGA-NSCLC and GSE50081 datasets was subjected to consensus clustering analysis. The correlation of ARGs expression with the prognosis and clinicopathological parameters of NSCLC was further evaluated. To construct a prognostic model, LASSO regression analysis and multivariate COX analysis were implemented for gene screening. The resulting model accurately estimated the risk of disease development or specific outcomes in NSCLC patients based on various predictive variables, including prognosis and clinicopathological parameters (age, sex, TMN stage, etc.) [56–58]. Survival curves showed that patients in the high-risk group had a lower overall survival and poorer prognosis. Additional analyses, such as DCA analysis, ROC analysis, ratio plot of clinicopathological parameters, and heatmap, further validated the significant correlation between ARG expression, clinical variables, and the prognosis of NSCLC patients. ROC and 3DPCA analysis preliminarily verified that the prognosis model has good stability. A nomogram, which is a visual graphical expression mode, was developed. It calculated scores based on individual predictor variable values and determined the risk level or survival probability of an event [59]. The results proved that the risk score derived from the nomogram served as an independent prognostic factor. Finally, the same calculation methodology was applied to the GSE30219 and GSE68465 cohorts to validate the model. Once again, the results confirmed the stability of the model.

The risk score serve as an independent prognostic factor for NSCLC. Prognostic risk genes may become tumor markers and therapeutic targets for the precise diagnosis and treatment of NSCLC in the future. In addition, further verification through in vitro cell experiments is needed to consolidate their role as tumor biomarkers [60]. Among the identified ARGs, ABL1 is involved in crucial processes related to cell growth and survival, including cell motility, adhesion, receptor endocytosis, autophagy, and apoptosis pathways. While primarily known as an oncogene associated with leukemia, it has also been reported to be associated with lung, bladder, and gastric cancers [61]. APOC3 is the protein component of triglyceride-rich lipoproteins. It promotes the assembly and secretion of very low-density lipoprotein 1 within cells and inhibits hydrolysis and clearance of triglyceride-rich lipoproteins outside cells [62, 63]. APOC3 has been identified as a biomarker in several malignancies, including hepatocellular carcinoma and colorectal cancer [64]. CDK1 can regulate the centrosome cycle and mitosis initiation, which is of great significance in the control of eukaryotic cell cycle, and the upregulation of CDK1 is closely related to the prognosis of various malignant tumors [65]. As a key transcription factor, CEBPB

regulates the expression of immune and inflammatory responses and plays a major role in immune responses such as CD4+T cell responses and granuloma formation. PDGFB is a growth factor that plays an important role in the regulation of cell proliferation, cell migration and chemotaxis. Diseases associated with PDGFB include dermatofibrosarcoma protuberans and idiopathic calcification of the basal ganglia. YWHAZ is upregulated in various cancers and acts as an oncogene in various cellular events, including hepatocellular carcinoma, colorectal cancer and lung cancer [66]. Based on qPCR in cell lines and extensive literature review, CEBPA was selected as the main focus for further research. Knockdown of CEBPA significantly reduced the mRNA and protein expression levels of CEBPB, YWHAZ, ABL1 and CDK1 in H1650 and A549 cells. To explore the potential biological functions of CEBPA in NSCLC cells, CEBPA siRNA was introduced into A549 and H1650 cells. The knockdown of CEBPA significantly reduced mRNA and protein levels in NSCLC cells as confirmed by qPCR and Western blot. The CCK-8 assay demonstrated a substantial decrease in the proliferation activity of NSCLC cell lines. EdU assay further confirmed that knockdown of CEBPA inhibited the proliferation of H1650 and A549 cells. Transwell and Matrigel Transwell assays revealed weakened migration and invasion of NSCLC cells upon knockdown of CEBPA. These results indicate that siRNA knockdown of CEBPA significantly inhibits NSCLC cell proliferation, migration, and invasion. Next, the overexpression plasmid was transduced into H1650 and A549 cells. qPCR and WB showed that CEBPA mRNA and protein expression levels were significantly up-regulated after OE-CEBPA. CCK-8 and EdU detection experiments showed that overexpression of CEBPA promoted cell proliferation. Transwell experiments showed that overexpression of CEBPA accelerated the migration and invasion of H1650 and A549 cells. This suggests that overexpression of CEBPA accelerates the proliferation, migration, and invasion of NSCLC cells. Consequently, CEBPA can be considered as a tumor biomarker to guide the diagnosis and treatment of NSCLC.

The TIME plays a crucial role in the initiation and progression of tumors. In this study, the ESTIMATE algorithm was first used to perform matrix score, immune score, and ESTIMATE score on patients in two different risk groups. Interestingly, it was found that only the immune score showed significant differences between the groups. Further analysis using ssGSEA evaluated the infiltration levels of CEBPA in 13 types of immune cells. The results indicated that the low-risk group exhibited higher immune scores. In recent years, T cells and B cells have emerged as key players in the tumor microenvironment. T cells have been identified as clinical biomarkers and have a significant impact on the prognosis of NSCLC [67, 68]. In early stages of NSCLC, B cells exhibit an inhibitory effect on cancer cell growth, while in advanced stages, they promote cell growth. mIHC was performed, revealing a significantly increased number of CD3+CD4+, CD3+CD8+, and CD20+cells in the high CEBPA expression group compared to the low expression group. Overall, in NSCLC, CEBPA is highly expressed in tumor cells, promoting their proliferation and migration, thereby facilitating tumor progression. The mIHC results demonstrated the colocalization of CEBPA with immune cell markers, indicating that T cells recognized and bound to tumor cells, leading to this colocalization phenomenon. However, the immune cells attracted by the tumor cells do not necessarily kill the tumor cells. While immune cells recognize and target tumor cells, their killing ability is inhibited by some immunosuppressive molecules such as PD1 and LAG3 [69–71]. Additionally, immune cells (e.g., macrophages) can create an immunosuppressive microenvironment, further inhibiting T cell-mediated tumor killing [72, 73].

In summary, this study conducted a comprehensive analysis of ARGs expression in NSCLC patients, identifying seven prognostic risk genes and constructing a prognostic risk model. Through in vitro experiments, it was found that CEBPA expression was significantly upregulated in NSCLC cells. Knockdown of CEBPA inhibited cell proliferation, migration, and invasion, while overexpression of CEBPA promoted these processes. Immunological correlation analysis showed that the low-risk group had higher immune scores. The colocalization of CEBPA with immune cell markers in NSCLC suggests its important role in the tumor microenvironment.

The potential clinical significance of this study is substantial. Firstly, the constructed prognostic risk model can help clinicians more accurately predict the prognosis of NSCLC patients and make personalized management and treatment decisions based on the risk scores. Secondly, key genes such as CEBPA, identified as potential tumor biomarkers and therapeutic targets, can guide the diagnosis and treatment strategies for NSCLC. Targeting these genes may lead to the development of new therapeutic approaches, improving patient prognosis and survival rates. Additionally, understanding the specific roles and mechanisms of these genes in NSCLC can contribute to the development of new immunotherapies, enhancing tumor immune response and ultimately improving treatment outcomes.

Despite the significant findings, this study has some limitations. Firstly, the specific molecular mechanisms of ARGs in the occurrence and development of NSCLC have not been deeply investigated. Secondly, the specific roles of ARGs in the immune microenvironment need further exploration. Future research should focus on elucidating the detailed mechanisms of these genes in tumor

progression and immune response, and further validate their effectiveness and mechanisms as tumor biomarkers and therapeutic targets through more in vitro and in vivo experiments.

Conclusions

The focus of this study was to identify the molecular subtypes of ARGs and develop a prognostic risk model.The risk model was found to be associated with NSCLC prognosis, clinicopathological parameters, immune microenvironment, and biological function. Specifically, CEBPA can serve as a tumor marker and immune target to guide the diagnosis and immunotherapy of NSCLC.

Abbreviations

NSCLC	Non-small cell lung cancer
ARGs	Aging-related genes
TIME	Tumor immune microenvironment
HAGR	Human aging gene repository
TCGA	The cancer genome atlas database
GEO	Gene expression omnibus database
LASSO	Least absolute shrinkage and selection operator
mIHC	Multiplex immunohistochemistry
AUC	Under the curve
OS	Overall survival
ssGSEA	Single-sample gene-set enrichment analysis
DEGs	Differentially expressed genes
DCA	Decision curve analysis
ROC	Receiver operating characteristic
HR	Hazard ratio
PCA	Principal component analysis

Supplementary Information

The online version contains supplementary material available at https://doi.org/10.1186/s12935-024-03457-4.

Supplementary Material 1

Acknowledgements

Not applicable.

Author contributions

J.Z., X.Z. and C.S. wrote the main manuscript text. Q.L. and Y.J. design the subject, X.C. and P.S. control experimental quality, Y.J., T.W. and J.C. analysis data and funding acquisition. All authors reviewed the manuscript.

Funding

This project was supported by grants from Wu Jinping Medical Foundation (HXKT20221037), National Science Fund subsidized project (82300412), Nantong University Affiliated Hospital doctoral research start-up fund project (Tdb2005), and Postgraduate Research & Practice Innovation Program of Jiangsu Province (KYCX24_3594).

Data availability

No datasets were generated or analysed during the current study.

Declarations

Ethics approval and consent to participate

All tissue samples involved in this study were obtained from paraffin-embedded surgical specimens of patients with previous NSCLC, and informed consent was signed and obtained. In order to protect the privacy of individuals, all personal details are not obtained. This project was approved by the Ethics Committee of the Affiliated Hospital of Nantong University (Number: 2023-L017).

Consent for publication

Not applicable.

Competing interests

The authors declare no competing interests.

Author details

[1]Department of Thoracic Surgery, Affiliated Hospital of Nantong University, Medical School of Nantong University, Nantong, China
[2]Department of Radiotherapy and Oncology, Affiliated Kunshan Hospital of Jiangsu University, Kunshan, China
[3]Cancer Immunotherapy Center, Cancer Research Institute, Xuzhou Medical University, Xuzhou, China
[4]Department of Burn and Plastic Surgery, Affiliated Hospital of Nantong University, Medical School of Nantong University, Nantong, China
[5]School of Medicine, Nantong University, Nantong, China
[6]Department of Clinical Biobank, The Institute of Oncology, Affiliated Hospital of Nantong University, Nantong, China
[7]Department of Rheumatology, Affiliated Hospital of Nantong University, Medical School of Nantong University, Nantong, China

Received: 22 February 2024 / Accepted: 20 July 2024
Published online: 27 July 2024

References

1. Torre LA, Bray F, Siegel RL, Ferlay J, Lortet-Tieulent J, Jemal A. Global cancer statistics, 2012. CA Cancer J Clin. 2015;65(2):87–108.
2. Ferlay J, Soerjomataram I, Dikshit R, Eser S, Mathers C, Rebelo M, Parkin DM, Forman D, Bray F. Cancer incidence and mortality worldwide: sources, methods and major patterns in GLOBOCAN 2012. Int J Cancer. 2015;136(5):E359–386.
3. Siegel RL, Miller KD, Jemal A. Cancer statistics, 2018. CA Cancer J Clin. 2018;68(1):7–30.
4. Bray F, Ferlay J, Soerjomataram I, Siegel RL, Torre LA, Jemal A. Global cancer statistics 2018: GLOBOCAN estimates of incidence and mortality worldwide for 36 cancers in 185 countries. CA Cancer J Clin. 2018;68(6):394–424.
5. Ettinger DS, Akerley W, Borghaei H, Chang AC, Cheney RT, Chirieac LR, Amico D TA, Demmy TL, Govindan R, Grannis FW, Jr., et al. Non-small cell lung cancer, version 2.2013. J Natl Compr Canc Netw. 2013;11(6):645–53. quiz 653.
6. Bai Y, Liu X, Qi X, Liu X, Peng F, Li H, Fu H, Pei S, Chen L, Chi X, et al. PDIA6 modulates apoptosis and autophagy of non-small cell lung cancer cells via the MAP4K1/JNK signaling pathway. EBioMedicine. 2019;42:311–25.
7. Bica-Pop C, Cojocneanu-Petric R, Magdo L, Raduly L, Gulei D, Berindan-Neagoe I. Overview upon miR-21 in lung cancer: focus on NSCLC. Cell Mol Life Sci. 2018;75(19):3539–51.
8. Li Y, Gu J, Xu F, Zhu Q, Ge D, Lu C. Transcriptomic and functional network features of lung squamous cell carcinoma through integrative analysis of GEO and TCGA data. Sci Rep. 2018;8(1):15834.
9. Zuo S, Wei M, Zhang H, Chen A, Wu J, Wei J, Dong J. A robust six-gene prognostic signature for prediction of both disease-free and overall survival in non-small cell lung cancer. J Transl Med. 2019;17(1):152.
10. Zhang Y, Yan Y, Ning N, Shen Z, Ye Y. A signature of 24 aging–related gene pairs predict overall survival in gastric cancer. Biomed Eng Online. 2021;20(1):35.
11. He S, Sharpless NE. Senescence in Health and Disease. Cell. 2017;169(6):1000–11.
12. Johnson SC, Rabinovitch PS, Kaeberlein M. mTOR is a key modulator of ageing and age-related disease. Nature. 2013;493(7432):338–45.
13. Ko LJ, Prives C. p53: puzzle and paradigm. Genes Dev. 1996;10(9):1054–72.
14. Calcinotto A, Kohli J, Zagato E, Pellegrini L, Demaria M, Alimonti A. Cellular Senescence: aging, Cancer, and Injury. Physiol Rev. 2019;99(2):1047–78.
15. Lee S, Schmitt CA. The dynamic nature of senescence in cancer. Nat Cell Biol. 2019;21(1):94–101.
16. Galluzzi L, Vitale I, Aaronson SA, Abrams JM, Adam D, Agostinis P, Alnemri ES, Altucci L, Amelio I, Andrews DW, et al. Molecular mechanisms of cell death: recommendations of the nomenclature Committee on Cell Death 2018. Cell Death Differ. 2018;25(3):486–541.

17. Xu Q, Chen Y. An aging-related gene signature-based model for risk stratification and prognosis prediction in Lung Adenocarcinoma. Front Cell Dev Biol. 2021;9:685379.
18. Kolar J, Mazumdarova K, Boudik F, Suntychova M, Chlup J, Ort J, Pick P. [Pulmonary edema and cardiogenic shock as a complication following cardioversion]. Vnitr Lek. 1976;22(4):380–9.
19. van Barjesteh S, Erpelinck C, Meijer J, van Oosterhoud S, van Putten WL, Valk PJ, Berna Beverloo H, Tenen DG, Lowenberg B, Delwel R. Biallelic mutations in the CEBPA gene and low CEBPA expression levels as prognostic markers in intermediate-risk AML. Hematol J. 2003;4(1):31–40.
20. Pabst T, Mueller BU. Complexity of CEBPA dysregulation in human acute myeloid leukemia. Clin Cancer Res. 2009;15(17):5303–7.
21. Roma-Rodrigues C, Mendes R, Baptista PV, Fernandes AR. Targeting Tumor Microenvironment for Cancer Therapy. Int J Mol Sci 2019, 20(4).
22. Zeng D, Li M, Zhou R, Zhang J, Sun H, Shi M, Bin J, Liao Y, Rao J, Liao W. Tumor Microenvironment characterization in gastric Cancer identifies prognostic and immunotherapeutically relevant Gene signatures. Cancer Immunol Res. 2019;7(5):737–50.
23. Hinshaw DC, Shevde LA. The Tumor Microenvironment innately modulates Cancer Progression. Cancer Res. 2019;79(18):4557–66.
24. Chen J, Tan Y, Sun F, Hou L, Zhang C, Ge T, Yu H, Wu C, Zhu Y, Duan L, et al. Single-cell transcriptome and antigen-immunoglobin analysis reveals the diversity of B cells in non-small cell lung cancer. Genome Biol. 2020;21(1):152.
25. Peng H, Wu X, Zhong R, Yu T, Cai X, Liu J, Wen Y, Ao Y, Chen J, Li Y, et al. Profiling Tumor Immune Microenvironment of Non-small Cell Lung Cancer using multiplex immunofluorescence. Front Immunol. 2021;12:750046.
26. Chu PG, Arber DA. CD79: a review. Appl Immunohistochem Mol Morphol. 2001;9(2):97–106.
27. Wei J, Chen P, Gupta P, Ott M, Zamler D, Kassab C, Bhat KP, Curran MA, de Groot JF, Heimberger AB. Immune biology of glioma-associated macrophages and microglia: functional and therapeutic implications. Neuro Oncol. 2020;22(2):180–94.
28. Iasonos A, Schrag D, Raj GV, Panageas KS. How to build and interpret a nomogram for cancer prognosis. J Clin Oncol. 2008;26(8):1364–70.
29. Tang D, Jiang H, Li Z, Gao W, Sun Y. The mechanism of ABL1 upregulating the expression of PD-L1 and the therapeutic effect of PD-L1 and STAT3 inhibitors in lung adenocarcinoma. Neoplasma. 2021;68(3):472–81.
30. Gu JJ, Rouse C, Xu X, Wang J, Onaitis MW, Pendergast AM. Inactivation of ABL kinases suppresses non-small cell lung cancer metastasis. JCI Insight. 2016;1(21):e89647.
31. Mano Y, Takahashi K, Ishikawa N, Takano A, Yasui W, Inai K, Nishimura H, Tsuchiya E, Nakamura Y, Daigo Y. Fibroblast growth factor receptor 1 oncogene partner as a novel prognostic biomarker and therapeutic target for lung cancer. Cancer Sci. 2007;98(12):1902–13.
32. Testoni E, Stephenson NL, Torres-Ayuso P, Marusiak AA, Trotter EW, Hudson A, Hodgkinson CL, Morrow CJ, Dive C, Brognard J. Somatically mutated ABL1 is an actionable and essential NSCLC survival gene. EMBO Mol Med. 2016;8(2):105–16.
33. Snaddon J, Smith ML, Neat M, Cambal-Parrales M, Dixon-McIver A, Arch R, Amess JA, Rohatiner AZ, Lister TA, Fitzgibbon J. Mutations of CEBPA in acute myeloid leukemia FAB types M1 and M2. Genes Chromosomes Cancer. 2003;37(1):72–8.
34. Pabst T, Mueller BU, Zhang P, Radomska HS, Narravula S, Schnittger S, Behre G, Hiddemann W, Tenen DG. Dominant-negative mutations of CEBPA, encoding CCAAT/enhancer binding protein-alpha (C/EBPalpha), in acute myeloid leukemia. Nat Genet. 2001;27(3):263–70.
35. Fuchs O, Kostecka A, Provaznikova D, Krasna B, Kotlin R, Stankova M, Kobylka P, Dostalova G, Zeman M, Chochola M. CCAAT/enhancer-binding protein alpha (CEBPA) polymorphisms and mutations in healthy individuals and in patients with peripheral artery disease, ischaemic heart disease and hyperlipidaemia. Folia Biol (Praha). 2010;56(2):51–7.
36. Zahnow CA. CCAAT/enhancer binding proteins in normal mammary development and breast cancer. Breast Cancer Res. 2002;4(3):113–21.
37. Pabst T, Mueller BU. Transcriptional dysregulation during myeloid transformation in AML. Oncogene. 2007;26(47):6829–37.
38. Johnson N, Cai D, Kennedy RD, Pathania S, Arora M, Li YC, D'Andrea AD, Parvin JD, Shapiro GI. Cdk1 participates in BRCA1-dependent S phase checkpoint control in response to DNA damage. Mol Cell. 2009;35(3):327–39.
39. Duma N, Santana-Davila R, Molina JR. Non-small Cell Lung Cancer: Epidemiology, Screening, diagnosis, and treatment. Mayo Clin Proc. 2019;94(8):1623–40.
40. Wang M, Herbst RS, Boshoff C. Toward personalized treatment approaches for non-small-cell lung cancer. Nat Med. 2021;27(8):1345–56.
41. Chen P, Liu Y, Wen Y, Zhou C. Non-small cell lung cancer in China. Cancer Commun (Lond). 2022;42(10):937–70.
42. Lindskog C, Edlund K, Mattsson JS, Micke P. Immunohistochemistry-based prognostic biomarkers in NSCLC: novel findings on the road to clinical use? Expert Rev Mol Diagn. 2015;15(4):471–90.
43. Seban RD, Assie JB, Giroux-Leprieur E, Massiani MA, Bonardel G, Chouaid C, Deleval N, Richard C, Mezquita L, Girard N, et al. Prognostic value of inflammatory response biomarkers using peripheral blood and [18F]-FDG PET/CT in advanced NSCLC patients treated with first-line chemo- or immunotherapy. Lung Cancer. 2021;159:45–55.
44. Yancik R. Cancer burden in the aged: an epidemiologic and demographic overview. Cancer. 1997;80(7):1273–83.
45. Miller KD, Nogueira L, Devasia T, Mariotto AB, Yabroff KR, Jemal A, Kramer J, Siegel RL. Cancer treatment and survivorship statistics, 2022. CA Cancer J Clin. 2022;72(5):409–36.
46. Gonzalez-Aragoneses F, Moreno-Mata N, Simon-Adiego C, Penalver-Pascual R, Gonzalez-Casaurran G, Perea LA. Lung cancer surgery in the elderly. Crit Rev Oncol Hematol. 2009;71(3):266–71.
47. Kendal WS. Dying with cancer: the influence of age, comorbidity, and cancer site. Cancer. 2008;112(6):1354–62.
48. Hanahan D, Weinberg RA. The hallmarks of cancer. Cell. 2000;100(1):57–70.
49. Zinger A, Cho WC, Ben-Yehuda A. Cancer and Aging - the inflammatory connection. Aging Dis. 2017;8(5):611–27.
50. Serrano M. Unraveling the links between cancer and aging. Carcinogenesis. 2016;37(2):107.
51. Finkel T, Serrano M, Blasco MA. The common biology of cancer and ageing. Nature. 2007;448(7155):767–74.
52. Reuter S, Gupta SC, Chaturvedi MM, Aggarwal BB. Oxidative stress, inflammation, and cancer: how are they linked? Free Radic Biol Med. 2010;49(11):1603–16.
53. Trachootham D, Lu W, Ogasawara MA, Nilsa RD, Huang P. Redox regulation of cell survival. Antioxid Redox Signal. 2008;10(8):1343–74.
54. Pawelec G, Derhovanessian E, Larbi A. Immunosenescence and cancer. Crit Rev Oncol Hematol. 2010;75(2):165–72.
55. Fares CM, Van Allen EM, Drake CG, Allison JP, Hu-Lieskovan S. Mechanisms of resistance to Immune Checkpoint Blockade: why does checkpoint inhibitor immunotherapy not work for all patients? Am Soc Clin Oncol Educ Book. 2019;39:147–64.
56. Hum A, Wong YKY, Yee CM, Lee CS, Wu HY, Koh MYH. PROgnostic model for Advanced Cancer (PRO-MAC). BMJ Support Palliat Care. 2020;10(4):e34.
57. Hoesseini A, van Leeuwen N, Sewnaik A, Steyerberg EW, Baatenburg de Jong RJ, Lingsma HF, Offerman MPJ. Key aspects of Prognostic Model Development and Interpretation from a clinical perspective. JAMA Otolaryngol Head Neck Surg. 2022;148(2):180–6.
58. Zhu J, Jiang Y, Wang T, Wu A, Zhou T, Zhang A, Tang Y, Shen Z, Wang J, Zhou H et al. Integrative Analysis of m6A RNA Methylation Regulators and the Tumor Immune Microenvironment in Non-Small-Cell Lung Cancer. *Dis Markers* 2022, 2022:2989200.
59. Park SY. Nomogram: an analogue tool to deliver digital knowledge. J Thorac Cardiovasc Surg. 2018;155(4):1793.
60. Zhang X, Feng H, Li Z, Li D, Liu S, Huang H, Li M. Application of weighted gene co-expression network analysis to identify key modules and hub genes in oral squamous cell carcinoma tumorigenesis. Onco Targets Ther. 2018;11:6001–21.
61. Kim MH, Yang GE, Jeong MS, Mun JY, Lee SY, Nam JK, Choi YH, Kim TN, Leem SH. VNTR polymorphism in the breakpoint region of ABL1 and susceptibility to bladder cancer. BMC Med Genomics. 2021;14(1):121.
62. Chan DC, Chen MM, Ooi EM, Watts GF. An ABC of apolipoprotein C-III: a clinically useful new cardiovascular risk factor? Int J Clin Pract. 2008;62(5):799–809.
63. Yao Z, Wang Y. Apolipoprotein C-III and hepatic triglyceride-rich lipoprotein production. Curr Opin Lipidol. 2012;23(3):206–12.
64. Wang X, Gong Y, Deng T, Zhang L, Liao X, Han C, Yang C, Huang J, Wang Q, Song X, et al. Diagnostic and prognostic significance of mRNA expressions of apolipoprotein A and C family genes in hepatitis B virus-related hepatocellular carcinoma. J Cell Biochem. 2019;120(10):18246–65.
65. Li M, He F, Zhang Z, Xiang Z, Hu D. CDK1 serves as a potential prognostic biomarker and target for lung cancer. J Int Med Res. 2020;48(2):300060519897508.
66. Wang W, Zhang L, Wang Y, Ding Y, Chen T, Wang Y, Wang H, Li Y, Duan K, Chen S, et al. Involvement of miR-451 in resistance to paclitaxel by regulating YWHAZ in breast cancer. Cell Death Dis. 2017;8(10):e3071.

67. Hanada KI, Zhao C, Gil-Hoyos R, Gartner JJ, Chow-Parmer C, Lowery FJ, Krishna S, Prickett TD, Kivitz S, Parkhurst MR, et al. A phenotypic signature that identifies neoantigen-reactive T cells in fresh human lung cancers. Cancer Cell. 2022;40(5):479–e493476.
68. Guo X, Zhang Y, Zheng L, Zheng C, Song J, Zhang Q, Kang B, Liu Z, Jin L, Xing R, et al. Global characterization of T cells in non-small-cell lung cancer by single-cell sequencing. Nat Med. 2018;24(7):978–85.
69. Wang J, Sanmamed MF, Datar I, Su TT, Ji L, Sun J, Chen L, Chen Y, Zhu G, Yin W, et al. Fibrinogen-like protein 1 is a major Immune Inhibitory ligand of LAG-3. Cell. 2019;176(1–2):334–47. e312.
70. Park JV, Chandra R, Cai L, Ganguly D, Li H, Toombs JE, Girard L, Brekken RA, Minna JD. Tumor cells modulate macrophage phenotype in a Novel in Vitro Co-culture Model of the NSCLC Tumor Microenvironment. J Thorac Oncol. 2022;17(10):1178–91.
71. Arner EN, Rathmell JC. Metabolic programming and immune suppression in the tumor microenvironment. Cancer Cell. 2023;41(3):421–33.
72. LaMarche NM, Hegde S, Park MD, Maier BB, Troncoso L, Le Berichel J, Hamon P, Belabed M, Mattiuz R, Hennequin C, et al. An IL-4 signalling axis in bone marrow drives pro-tumorigenic myelopoiesis. Nature. 2024;625(7993):166–74.
73. Casanova-Acebes M, Dalla E, Leader AM, LeBerichel J, Nikolic J, Morales BM, Brown M, Chang C, Troncoso L, Chen ST, et al. Tissue-resident macrophages provide a pro-tumorigenic niche to early NSCLC cells. Nature. 2021;595(7868):578–84.

Publisher's Note